Title

Abbreviated scan protocols to capture 18F-FDG kinetics for long axial FOV PET scanners.

Journal

European Journal of Nuclear Medicine and Molecular Imaging, 49(9)

Authors

Viswanath, Varsha

Sari, Hasan

Pantel, Austin

et al.

Publication Date

2022-07-01

DOI

10.1007/s00259-022-05747-3

Peer reviewed

HHS Public Access

Author manuscript

Eur J Nucl Med Mol Imaging. Author manuscript; available in PMC 2023 December 04.

Published in final edited form as:

Eur J Nucl Med Mol Imaging. 2022 July ; 49(9): 3215–3225. doi:10.1007/s00259-022-05747-3.

Abbreviated scan protocols to capture ^{18}F-FDG kinetics for long axial FOV PET scanners

Varsha Viswanath[1], **Hasan Sari**[2,3], **Austin R. Pantel**[1], **Maurizio Conti**[4], **Margaret E. Daube-Witherspoon**[1], **Clemens Mingels**[3], **Ian Alberts**[3], **Lars Eriksson**[4,5], **Kuangyu Shi**[3], **Axel Rominger**[3], **Joel S. Karp**[1]

[1]Department of Radiology, Perelman School of Medicine, University of Pennsylvania, Philadelphia, PA, USA

[2]Advanced Clinical Imaging Technology, Siemens Healthcare AG, Lausanne, Switzerland

[3]Department of Nuclear Medicine, Inselspital, Bern University Hospital, University of Bern, Freiburgstrasse, 18, 3010 Bern, Switzerland

[4]Siemens Medical Solutions, USA Inc., Knoxville, TN, USA

[5]Department of Oncology and Pathology, Medical Radiation Physics, Karolinska Institutet, Stockholm, Sweden

Abstract

Purpose—Kinetic parameters from dynamic ^{18}F-fluorodeoxyglucose (FDG) imaging offer complementary insights to the study of disease compared to static clinical imaging. However, dynamic imaging protocols are cumbersome due to the long acquisition time. Long axial field-of-view (LAFOV) PET scanners (> 70 cm) have two advantages for dynamic imaging over clinical PET scanners with a standard axial field-of-view (SAFOV; 16–30 cm). The large axial coverage enables multiorgan dynamic imaging in a single bed position, and the high sensitivity may enable clinically routine abbreviated dynamic imaging protocols.

Methods—In this work, we studied two abbreviated protocols using data from a 65-min dynamic ^{18}F-FDG scan: (A) dynamic imaging immediately post-injection (p.i.) for variable durations, and (B) dynamic imaging immediately p.i. for variable durations plus a 1-h p.i. (5-min-long) datapoint. Nine cancer patients were imaged on the Biograph Vision Quadra (Siemens Healthineers). Time-activity curves over the lesions (N = 39) were fitted using the Patlak graphical analysis and a 2-tissue-compartment (2C, $k_4 = 0$) model for variable scan durations (5–60 min). Kinetic parameters from the complete dataset served as the reference. Lesions from all cancers were grouped into low, medium, and high flux groups, and bias and precision of K_i (Patlak) and K_i, K_1, k_2, and k_3 (2C) were calculated for each group.

✉Margaret E. Daube-Witherspoon, daubewit@pennmedicine.upenn.edu.

Competing interests HS is a full-time employee of Siemens Healthineers AG. LE and MC are full time employees of Siemens Medical Solutions USA, Inc. AR has received research support and speaker honoraria from Siemens Healthineers. ILA declares no conflict of interest. The other authors have no relevant financial or non-financial interests to disclose.

Ethics approval The local Institutional Review Board approved the study (KEK 2019–02193) and written informed consent was obtained from all patients. The study was performed in accordance with the declaration of Helsinki.

Results—Using only early dynamic data with the 2C (or Patlak) model, accurate quantification of K_i required at least 50 (or 55) min of dynamic data for low flux lesions, at least 30 (or 40) min for medium flux lesions, and at least 15 (or 20) min for high flux lesions to achieve both 10% bias and precision. The addition of the final (5-min) datapoint allowed for accurate quantification of K_i with a bias and precision of 10% using only 10–15 min of early dynamic data for either model.

Conclusion—Dynamic imaging for 10–15 min immediately p.i. followed by a 5-min scan at 1-h p.i can accurately and precisely quantify ^{18}F-FDG on a long axial FOV scanner, potentially allowing for more widespread use of dynamic ^{18}F-FDG imaging.

Keywords

FDG; Dynamic imaging; ^{18}F-FDG flux

Introduction

Dynamic imaging of [^{18}F]-fluorodeoxyglucose (FDG) offers valuable information about the time course of uptake. The standardized uptake value (SUV) is a simplification of ^{18}F-FDG flux (K_i), implemented in the clinic to minimize scan durations, optimize clinical workflows, and simplify image reconstruction. SUV is a semi-quantitative metric and allows for consistent and reproducible clinical decision-making both within and across institutions [1–4]. Despite its widespread use, there are still valid concerns to using SUV as a metric to quantify ^{18}F-FDG uptake in lesions. Standard-of-care (SOC) static images are typically acquired around 1 h post-injection (p.i.), when ^{18}F-FDG uptake in lesions is often still changing [5]. This change in uptake over time is inherently accounted for in kinetic modeling, as is tracer availability in the blood, which is poorly accounted for in the SUV calculation. Additionally, kinetic analysis of ^{18}F-FDG can estimate tracer delivery (K_1) to tissues. Tseng et al. studied a group of locally advanced breast cancer patients and showed that while ^{18}F-FDG flux decreased in both responsive and non-responsive groups, blood flow, as measured using ^{15}O-water, increased in non-responsive groups and decreased in responsive groups [6]. Although the clinical utility of K_i and K_1 has been well studied for breast cancer by researchers at the University of Washington [6–8], and some work has been done to correlate microparameters with cancer disease stages [9, 10], further work is necessary to understand the broader role of ^{18}F-FDG kinetic parameters in clinical cancer management.

Despite its demonstrated value, dynamic imaging is still a challenging protocol for many patients and institutions. For ^{18}F-FDG, the standard imaging duration is 1 h, which can be uncomfortable for patients, particularly for non-compliant or claustrophobic patients, resulting in motion during the scan. The long acquisition time negates the advantages of short duration scans using state-the-art digital scanners, potentially hampering the clinical routines of a busy nuclear medicine department [11, 12].

With standard axial field of view (SAFOV) scanners, dynamic imaging is typically done over a single bed position, limiting the ability to image tumors in multiple organs simultaneously and precluding generation of an image derived input function (IDIF) if a major vessel (e.g., left ventricle or aorta) is not within the axial field of view (AFOV).

To address this issue, dynamic imaging with continuous bed motion has been developed [13, 14]. Early imaging is done over the heart to get an accurate IDIF, followed by multiple passes of the body to capture the whole-body kinetics. However, this protocol results in temporally coarse data, which could lead to uncertainties during fitting. The lower sensitivity of SAFOV scanners coupled with the short frames required to capture fast kinetics immediately p.i. can result in noisy images that hinder accurate and precise kinetic analysis. Long AFOV (LAFOV) scanners (i.e., AFOV > 70 cm) can simultaneously image much of the whole body, while offering up to a 3 × increase in peak axial sensitivity [15]. The high sensitivity leads to low image noise of even short frames that translates to an improvement in kinetic parameter estimation [16].

There are currently three LAFOV scanner designs in operation: the United Imaging uEXPLORER (194-cm AFOV) at UC Davis and a number of sites throughout China [17], the PennPET Explorer (136-cm AFOV) at the University of Pennsylvania [18], and the Siemens Biograph Vision Quadra (106-cm AFOV) at the University of Bern [11, 19]. Thus far, UC Davis has implemented a parametric image reconstruction algorithm [20] with model selection based on Akaike information criterion [21] and studied the use of dual input functions in relevant organs [22]. Additionally, researchers at Siemens Healthineers have implemented parametric image generation using data from the Siemens Quadra and Patlak graphical analysis [23]. In prior work on SAFOV scanners, Strauss et al. studied abbreviated scan durations, ranging from 10- to 30-min-long dynamic scans using over 500 patients. Given a 90% variance, a 20-min early dynamic scan followed by a 1-h time point was required to accurately estimate kinetic parameters [24]. Most relevant to this work is the study by Wu et al., where seven ^{18}F-FDG patients were imaged on the uEXPLORER and K_i of lesions ($n = 26$) was estimated using two protocols: (1) dynamic imaging from 0 to 60 min and (2) dynamic imaging from 0 to 4 min plus a static image from 54–60 min p.i. Whereas Wu et al. showed similar K_i estimation across the two protocols and reconstructed parametric K_i images using only 10 min of dynamic data [25], we studied a range of abbreviated protocols, along with the impact of abbreviated imaging on both micro and macro kinetic parameters.

In this work, we take a methodical and rigorous quantitative approach to studying abbreviated scan protocols using ^{18}F-FDG patient data imaged on the Siemens Quadra. We hypothesize that a shortened dynamic scan protocol might improve clinical acceptability and utilization of parametric imaging data. The aim of this study was to evaluate the acceptability of two abbreviated scan protocols and use the bias and precision of flux (K_i) and delivery (K_1) estimates, along with the ^{18}F-FDG microparameters k_2 and k_3, to determine the optimal scan duration for each abbreviated scan protocol.

Methods

Data acquisition

Acquisition of these data has been previously described in [26]. Data-sets were prospectively acquired from nine cancer patients (including lymphoma, breast, lung, and gastric cancers) undergoing routine clinical PET/CT. Patients were injected with 170–400 MBq (4.6–10.8 mCi) of ^{18}F-FDG with dynamic imaging for 65 min on the Siemens Biograph Vision Quadra

at the University Hospital, Bern, Switzerland [19] (Table 1). A standardized body weight-adapted dose of 3.0 MBq/kg was applied, as per EANM guidelines [27]. This study was approved by the cantonal ethics committee, and all subjects provided informed consent for participation. Data were binned into 62 frames (2 × 10 s, 30 × 2 s, 4 × 10 s, 8 × 30 s, 4 × 60 s, 5 × 2 min, 9 × 5 min) and reconstructed using the manufacturer's default reconstruction method, which incorporates modeling of the point spread function + time-of-flight (PSF + TOF OSEM, 4 iterations × 5 subsets), followed by Gaussian post-filtering (2-mm FWHM) into 1.65 × 1.65 × 1.645 mm^3 voxels. Note that data acquisition was started 15 s before injection through a 150-cm long Heidelberger extension line; the initial two 10-s frames accommodated the delay in arrival of activity in the body.

Data analysis

All clinical scans were dual reported by an experienced resident and board-certified nuclear medicine physician. Lesions consistent with the patient's known oncological diagnosis were identified in PMOD (PMOD Technologies LLC, Zürich, Switzerland) by an experienced clinician at the University Hospital of Bern and spherical VOI were semi-automatically drawn over lesions, as follows. A large search region was manually drawn in MIM (MIM Software Inc, Beachwood, OH) to include the tumor while excluding other high-uptake regions. Using MIM, an automatic search was performed to find the maximum average uptake in a volume of interest (VOI) of a given sphere diameter, where the diameter was manually set to inscribe the lesion. This was done to avoid user bias when drawing VOI across lesions. Lesion diameters ranged from 4 to 28 mm with an average diameter of 10 mm.

Additionally, to compensate for motion, the VOI position was adjusted on a frame-by-frame basis by searching for the maximum VOI uptake (mean) in each of the last 10 frames (last 45 min). Only the last 10 frames were adjusted, where the lesion uptake was higher than the background. Because tumor uptake was lower than background in early frames, searching for the local maximum would have resulted in inaccurate VOI localization; therefore, the VOI location from the earliest frame with motion compensation applied (i.e., the frame at 15 min p.i) was used for all earlier frames, assuming minimal motion in those first 15 min.

A total of 39 lesions were used in the final analysis. A cylindrical VOI (10-mm diameter, 88 ± 21 mm long) was drawn in the descending aorta (i.e., between the aortic arch and the diaphragm) to measure the blood time-activity curve (TAC). All TAC were corrected for scan duration and radio-active decay, but no partial volume correction was applied. Prior to compartmental modeling, the IDIF was fit in PMOD to a line up to the peak and a tri-exponential following the peak. This fit curve was then used in the kinetic analysis.

Two abbreviated scan protocols were studied by retrospectively analyzing portions of the acquired 65-min dynamic studies (Fig. 1). Protocol A used early dynamic data only, starting at 0 min and ending at t min, where t ranged from 5 to 65 min. Protocol A had the advantage that, in application, it would require only a single imaging session and a single CT, allowing for ease of clinical workflow while negating the 1-h uptake time currently required for patients; however, it would not inherently include the 60-min p.i. SUV image that is used for regular clinical management. Protocol B used early dynamic data plus the final dynamic

frame, which corresponded to a static scan at 60 min p.i., typically used in the clinic. Data points that were used started at 0 min and ended at t min, where t ranged from 5 to 60 min, followed by the final 5-min frame from 60 to 65 min. Although much work has been done with dual-time-point FDG imaging and late FDG imaging past 1 h p.i. [28, 29], our data acquisition was constrained to a 65-min dynamic session; therefore, we were unable to assess the value of later final time points for kinetic parameter estimation. In practice, protocol B would inherently include the 60 min p.i. SUV image used clinically; however, it would require two imaging sessions, each with a CT for attenuation correction. Furthermore, while the position of VOI could be adjusted for any misalignment in lesion location between the early frames and the final frame, resultant images from the two imaging sessions would need to be registered to generate whole-body parametric images.

TAC of both the lesion and the IDIF were filtered to include only the desired time points for protocols A and B and were fit using PKIN (PMOD v4.1). TAC were analyzed using both Patlak graphical analysis [30] to quantify K_i and an irreversible 2-tissue-compartment (2C) model to quantify K_1 and K_i as well as the microparameters k_2 (efflux from the first tissue compartment) and k_3 (phosphorylation of hexokinase); the blood volume, v_B, and the delay time of the blood TAC were also fit. The start time (t*) for Patlak was defined based on a 10% error threshold, as is commonly done in PMOD [31], and was lesion dependent.

For each lesion, the bias of kinetic parameters from the abbreviated scans was calculated with respect to value estimated using the full 65-min dynamic dataset. Based on the flux from the 65-min fit, lesions were separated into low, medium, and high flux lesions, where low flux lesions had a K_i less than 0.02 ml/cm^3/min, medium flux lesions had a K_i between 0.02 and 0.04 ml/cm^3/min, and high flux lesions had a K_i greater than 0.04 ml/cm^3/min. The highest flux lesion had a K_i of 0.096 ml/cm^3/min. This categorization was based on the range of FDG flux values in literature at various sites [32–35] as well as prior work to quantify bias and precision of kinetic parameter estimation with data acquired on the PennPET Explorer [16]. Separation by flux was selected because flux reflects the count statistics of a lesion. A higher uptake lesion will have better count statistics and can potentially be more accurately quantified than a low flux lesion. The average and standard deviation of bias were calculated for each flux group, where the bias was measured as the average bias over all lesions in a given flux group and the precision was measured as the standard deviation of the bias over all lesions in that flux group. An alternative analysis could be to use the bias vs. scan duration data for each lesion individually to determine the minimum scan duration to achieve the desired bias and precision for a lesion and then average these scan durations over all lesions in a flux group. However, there was considerable variation among lesions (e.g., for some lesions, the bias or precision was always below the threshold for all scan durations studied), so we chose to use the average bias and precision over all lesions in a flux group to determine the minimum scan durations instead.

Results

SUV images of the final dynamic frame (5-min duration) from two representative patients are shown in Fig. 2. Lesions are located in various axial locations along the length of the

patient's body, necessitating imaging with a LAFOV scanner to capture the kinetics of all lesions as well as the descending aorta. Plots below the images show the TAC of lesions indicated with red arrows, showcasing the range of kinetics in a single patient. Image quality for both patients is superb, showcasing the high sensitivity of the Siemens Quadra.

Plotted in figures below are the average bias ± the standard deviation for each flux group and dynamic scan duration. In this work, we chose a threshold of 10% for both bias and standard deviation as an acceptable error in determining the minimum scan duration, following our prior work [16], while still maintaining good accuracy and precision for kinetic parameter estimation. In Table 2 (and later in Table 4), we report the scan durations corresponding to the 10% acceptance threshold, for both bias and standard deviation of kinetic parameters. Durations were interpolated to give the value at the 10% threshold, based on measured data points, and were rounded to the nearest minute. Because any threshold can be somewhat arbitrary, we also report scan durations corresponding to acceptance thresholds of 5 to 12.5% in Table 3 for bias and precision of K_i estimated using both Patlak analysis and the two-tissue-compartment model.

Figure 3 plots bias and standard deviation (i.e., precision) of flux (K_i) fit using the Patlak graphical analysis method. Using protocol A, the low, medium, and high flux lesions require scan times greater than 55, 39, and 19 min, respectively, to achieve a bias or precision of < 10%. Using early dynamic data plus a static scan at 60 min p.i. (protocol B), the bias exceeds 10% for scan durations shorter than 6, 12, and 13 min, respectively, and exceeds 5% for scan durations shorter than 15 min for all three fluxes. For dynamic scans as short as 10 min, the precision remains at 5% or lower. Tables 2A and 3 (top) summarize these findings.

Figure 4 depicts bias and precision of flux (K_i) fit using an irreversible 2C model. When fitting using only early dynamic data (protocol A), minimum dynamic scan durations of 49, 28, and 13 min are required for low, medium, and high flux lesions, respectively, to remain below a 10% threshold for both bias and precision. With the addition of the 5 min static data point (protocol B), scan durations shorter than 15 min are sufficient to maintain less than 10% bias and precision for all fluxes. Table 2B summarizes these findings. Table 3 illustrates the impact of the threshold on the scan durations needed to achieve that threshold in bias or precision.

Figure 5 shows the bias and precision of delivery (K_1) from the 2C model. K_1 has minimal bias and good precision using either early dynamic data only (protocol A) or dynamic plus static data (protocol B). Using protocol A, the bias in K_1 estimated using only a 10-min dynamic scan was 4.3 ± 8.4%, averaged over all fluxes. In comparison, the bias and precision using protocol B were − 0.9 ± 4.0%.

Figure 6 shows the bias and precision of estimating k_2 and k_3 using a 2C model for both protocols. Using protocol A, accurate and precise estimation of k_2 requires 50, 36, and 17 min of dynamic data for low, medium, and high flux lesions, respectively. Similarly, accurate and precise estimation of k_3 requires 55, 37, and 32 min of dynamic data, respectively, for low, medium, and high flux lesions. Using protocol B, low flux lesions require 20 min of data to precisely estimate k_2 but 45 min of dynamic data to precisely estimate k_3. For

medium and high flux lesions, however, k_2 can be accurately estimated using < 5 min of data, while accurate estimation of k_3 requires 12–16 min of dynamic data. These findings are summarized in Table 4.

Discussion

This work used datasets from 65-min-long ^{18}F-FDG PET/CT scans of cancer patients imaged on the Siemens Biograph Vision Quadra to study two abbreviated dynamic imaging protocols: protocol A, which uses only early dynamic data (0-t min p.i.), and protocol B, which uses early dynamic data plus a final 5-min frame (0-t min p.i. + 60–65 min p.i.).

We have previously shown that the high sensitivity of long AFOV scanners allows for improved estimation of kinetic parameters [16, 26], and this work leverages the high sensitivity of the Siemens Quadra to study abbreviated scan protocols. The Siemens Quadra has demonstrated the ability to obtain high count statistic scans with shorter acquisition times [36], and the axial length (1.06 m) of the Siemens Quadra allows for simultaneous dynamic imaging of multiple lesions in a single imaging session. This axial length covers most oncologically relevant regions without compromising temporal sampling, as is required when imaging using a SAFOV scanner. Although this work was done on a LAFOV system with high sensitivity, this does not preclude extending these methods to implement a similar protocol on a SAFOV system.

Estimation of flux using protocol A with either Patlak graphical analysis (Fig. 3) or a 2-tissue-compartment model (Fig. 4) shows high bias of low flux lesions for any abbreviated scan duration. Since the bias exceeds 10% at 40 min for both models (Table 2), this makes protocol A less practical for any cases with low flux lesions. Even though the bias of the medium flux lesions is much lower for abbreviated scans, the precision for shorter scans remains poor (> 20%). In fact, 39-min and 28-min dynamic scans are required to maintain 10% precision using Patlak and the 2C models, respectively, which would still be an impractical scan duration for a clinical protocol. The addition of the static 5-min scan (protocol B) greatly stabilizes estimation of flux using either Patlak or the 2C model. For lesions of any flux, a 10–15 min dynamic scan would maintain a bias less than 10% and a precision better than 5%. Additionally, a 10–15-min scan is on par with, or shorter than, current static SUV scan durations for SAFOV scanners. Also of note, the fluxes as measured by Patlak analysis and the two-tissue-compartment model were highly correlated.

As seen in Table 3, with protocol A, the precision of the flux estimate is the limiting factor in scan duration reduction for both Patlak analysis and the two-tissue-compartment model. As the desired bias or precision is tightened (lower threshold), the scan duration needed to achieve that level becomes even longer. With protocol B, the precision of the flux estimate is improved, and the desired bias becomes the limiting factor in shortening the duration of the early portion of the study. As with protocol A, a lower threshold (better bias or precision) necessitates longer scan durations of the early portion, although the impact is less pronounced than for protocol A; even 5% bias can be achieved for most cases with < 20 min with either Patlak graphical analysis or the two-tissue-compartment model. While a similar

analysis was not performed for the microparameters, k_2 and k_3, similar trends would be expected, based on Fig. 6.

Because estimation of delivery (K_1) depends on the early portion of the tumor TAC and the IDIF, it is not surprising that bias and precision of K_1 remain below 10% for even the shortest scan durations studied, regardless of the imaging protocol used (Fig. 5). However, the addition of the static data point (protocol B) does reduce the bias and improves the precision of K_1, most likely due to the increased stability in the fit afforded by the 60-min data point.

Finally, we also assessed the accuracy and precision of the microparameters, k_2 and k_3, with both abbreviated protocols. Using protocol A, medium and low flux lesions require 37 min and 55 min, respectively, for accurate estimation of either k_2 or k_3. While the precisions of k_2 and k_3 for low flux lesions estimated using protocol B are quite poor (> 15%) for shorter scan durations (< 15 min), the bias is still below 10% for 10–15-min scans. Additionally, estimation of k_2 and k_3 for medium and high flux lesions maintains a bias and precision of < 10% for 10–16-min dynamic scans. Overall, k_2 and k_3 can be well estimated for medium and high flux lesions, while low flux lesions have low bias but poor precision.

Results overall show improved bias and precision results for high and medium flux lesions compared to low flux lesions. This is reasonable since higher flux lesions will have better count statistics and therefore more stable fits compared to lower flux lesions. Results also showed that the addition of a static scan at 60 min p.i. (protocol B) improved both bias and precision for all range of fluxes. Overall, this work showed that using early dynamic data plus a static data point at 60 min p.i. (protocol B) resulted in improved bias and precision of kinetic parameter estimates for dynamic scans as short as 10–15 min (with a 10% threshold for bias and precision). Therefore, we recommend the scan protocol outlined in Fig. 7 where a patient would be imaged for 10–15 min dynamically p.i., followed by a break, then imaged for 5 min at 60 min p.i.

Although Wu et al. studied abbreviated dynamic FDG imaging using the uEXPLORER system, they only reported differences in K_i for one specific protocol [25]. In this present study, we report the first data for abbreviated scan protocols for the Siemens Biograph Vision Quadra, including an investigation of the bias and precision of K_i, K_1, k_2, and k_3 for a range of acquisition times and two different imaging protocols. Wu et al. compared dynamic imaging from 0 to 60 min with a second protocol that imaged from 0 to 4 min, followed by a 54–60 min p.i. scan. Their work showed that differences in K_i between their first and second protocols were no more than 0.005 ml/cm^3/min, a 12–30% bias depending on the mean K_i. In comparison, our work studied two protocols for a range of scan durations, quantified K_i using both Patlak and compartmental modeling, and studied the effect of various scan durations and protocols on microparameters k_2 and k_3. We also separated lesions into three flux groups and clearly showed that higher flux lesions performed better than lower flux lesions. Additionally, using protocol B, we showed a 10% bias in K_i with a 10–15-min dynamic scan and a roughly 20% bias with a 5-min dynamic scan. Finally, Wu et al. studied 26 lesions in seven patients, while our study utilized more lesions (n = 39) in 9 patients. In addition, while Strauss et al. found that a 20-min dynamic scan followed by a whole-body

scan at 60 min gave kinetic parameters with an accuracy (bias) of 90% on a SAFOV scanner [24], the higher sensitivity of the LAFOV system permits imaging for only 10–15 min with a 5-min scan at 60 min p.i. for comparable accuracy.

Although protocol B better estimates kinetic parameters compared to protocol A, protocol B has several potential practical drawbacks. The major drawback is the requirement for two imaging sessions, where additional patient handling might hamper a busy clinical workflow. The additional dose of the second low-dose CT is also of potential relevance, although the small additional radiation burden of a low-dose CT (~ 1 mSv) in comparison to the total radiation burden of the examination (5.7 mSv for 300 MBq of ^{18}F-FDG) is minimal [37]. Moreover, there is potential for reduction in injected activity afforded by LAFOV systems [36], and there are options to lower the radiation burden of two CTs on the patients, including using lower dose CTs, a CT-less reconstruction, or AI-based methods [38, 39]. Additionally, if one wishes to generate parametric images, which have been shown to provide better lesion contrast compared to SUV images [20, 29], the two scans from protocol B would need to be registered. There have been numerous methods proposed for motion correction/image registration in PET [40]; a data-driven approach, such as the centroid-of-distribution method [41], would be a likely candidate to incorporate into the clinical workflow.

As opposed to a fully dynamic 65-min protocol, our abbreviated scan protocol allows for either static imaging of 1–2 other patients or dynamic imaging of one other patient in the 45–50-min interim time between scans. Additionally, this dynamic protocol capitalizes on the high sensitivities of LAFOV scanner systems and the ability to image the entire torso in a single bed position to collect a 5-min static scan that can be read as a traditional clinical static PET/CT scan. Moreover, the total scan time of 15–20 min is comparable to the scan duration required with a SAFOV scanner. Finally, although not studied in this work, the timing of the final static SUV scan could be flexible depending on the clinical schedule or clinical indication. We were constrained by the 65-min dynamic acquisition in this study; however, other studies have clearly shown the benefit of late imaging [28], and this would be ripe for further study. SUV imaged at 2 h p.i. with a long AFOV scanner can take advantage of washout kinetics of normal tissues [42], although this may require adjusting a traditional clinical interpretation of FDG SUV. In contrast, dynamic imaging accounts for the time course and appropriately estimates flux.

This study analyzed a small number of patients (n = 9) but a larger number of lesions (n = 39) and represents the first experiences using parametric imaging protocols with the recently installed Siemens Quadra LAFOV PET/CT system. Further studies, potentially focused on individual cancer types or using SAFOV scanners, might explore further the optimal scan duration for different tumors or treatment protocols. Additionally, this paper used a 10% threshold to define acceptable bias and precision; however, if one were to tolerate a higher threshold for either bias or precision, the data presented here could be used to define even shorter imaging protocols. Furthermore, this work only tested kinetic analysis on tumor TAC and not TAC of normal tissues. If one were interested in obtaining parametric images, then this would need further evaluation. Finally, although this study was conducted with

^{18}F-FDG, future studies should extend the methodology demonstrated herein to different radiopharmaceuticals [43].

The protocol proposed in Fig. 7 includes a total of 15–20 min of imaging time, a vast improvement on current 1-h protocols required to measure FDG kinetics in the body. The typical 1-h protocol is uncomfortable for patients, especially older cancer patients, resulting in increased artifacts from patient motion during the scan and lower patient interest in such protocols overall. In our methods, we adjusted the placement of the VOI to correct for motion; however, the population of patients imaged had minimal motion. TAC were analyzed using the VOI that were not adjusted for motion, and results (not shown here) were similar to those obtained with motion-adjusted VOI. However, there is a necessity to assess and correct for motion, in cases where there is larger gross motion. Overall, the radically shorter imaging time will allow clinics to integrate dynamic FDG imaging into their workflow, possibly by delaying the static data point in protocol B, resulting in more widespread use, and a large database of kinetic FDG parameters for a range of diseases will inform how best to utilize such information for clinical disease management.

Conclusion

This paper tested two abbreviated dynamic imaging protocols for ^{18}F-FDG using data from the Siemens Biograph Quadra Vision, a long AFOV scanner. To maintain acceptable quantification of K_1 and K_i (both a bias and precision of 10%) while also allowing for measurement of SUV, we recommend a 10–15-min dynamic immediately p.i., followed by a 5-min static scan at 1 h p.i. This will also allow for estimation of k_2 and k_3, although the uncertainties of the biases and precisions depend on lesion flux. Such abbreviated protocols might be more practicable in a busy clinic and allow clinicians to study the interplay between K_i, K_1, k_2, and k_3 for a range of cancers to help guide cancer treatment and management in the future.

Funding

This work was supported by the following grants: NIH R01 CA225874 and NIH R01 C113941, along with a research contract between the University of Pennsylvania and Siemens Medical Solutions and a research agreement between Insel Gruppe AG, Bern, Switzerland, and Siemens Healthcare AG, Zürich, Switzerland.

References

1. Wahl RL, Jacene H, Kasamon Y, Lodge MA. From RECIST to PERCIST: evolving considerations for PET response criteria in solid tumors. J Nucl Med. 2009;50:122S–S150. [PubMed: 19403881]
2. Visser EP, Boerman OC, Oyen WJ. SUV: from silly useless value to smart uptake value. J Nucl Med. 2010;51:173–5. [PubMed: 20080897]
3. Lodge MA. Repeatability of SUV in oncologic ^{18}F-FDG PET. J Nucl Med. 2017;58:523–32. [PubMed: 28232605]
4. Aide N, Lasnon C, Veit-Haibach P, Sera T, Sattler B, Boellaard R. EANM/EARL harmonization strategies in PET quantification: from daily practice to multicentre oncological studies. Eur J Nucl Med Mol Imaging. 2017;44:17–31. 10.1007/s00259-017-3740-2.
5. Beaulieu S, Kinahan P, Tseng J, Dunnwald LK, Schubert EK, Pham P, et al. SUV varies with time after injection in ^{18}F-FDG PET of breast cancer: characterization and method to adjust for time differences. J Nucl Med. 2003;44:1044–50. [PubMed: 12843218]

6. Tseng J, Dunnwald LK, Schubert EK, Link JM, Minoshima S, Muzi M, et al. ^{18}F-FDG kinetics in locally advanced breast cancer: correlation with tumor blood flow and changes in response to neoadjuvant chemotherapy. J Nucl Med. 2004;45:1829–37. [PubMed: 15534051]
7. Doot RK, Kurland BF, Kinahan PE, Mankoff DA. Design considerations for using PET as a response measure in single site and multicenter clinical trials. Acad Radiol. 2012;19:184–90. [PubMed: 22104290]
8. Doot RK, McDonald ES, Mankoff DA. Role of PET quantitation in the monitoring of cancer response to treatment: review of approaches and human clinical trials. Clin Transl Imaging. 2014;2:295–303. [PubMed: 25229053]
9. Dimitrakopoulou-Strauss A, Strauss LG, Heichel T, Wu H, Burger C, Bernd L, et al. The role of quantitative ^{18}F-FDG PET studies for the differentiation of malignant and benign bone lesions. J Nucl Med. 2002;43:510–8. [PubMed: 11937595]
10. Dimitrakopoulou-Strauss A, Strauss LG, Schwarzbach M, Burger C, Heichel T, Willeke F, et al. Dynamic PET ^{18}F-FDG studies in patients with primary and recurrent soft-tissue sarcomas: impact on diagnosis and correlation with grading. J Nucl Med. 2001;42:713–20. [PubMed: 11337565]
11. Alberts I, Prenosil G, Mingels C, Bohn KP, Viscione M, Sari H, et al. Feasibility of late acquisition [^{68}Ga]Ga-PSMA-11 PET/CT using a long axial field-of-view PET/CT scanner for the diagnosis of recurrent prostate cancer-first clinical experiences. Eur J Nucl Med Mol Imaging. 2021;48:4456–62. 10.1007/s00259-021-05438-5. [PubMed: 34155538]
12. Alberts I, Sachpekidis C, Prenosil G, Viscione M, Bohn KP, Mingels C, et al. Digital PET/CT allows for shorter acquisition protocols or reduced radiopharmaceutical dose in [18F]-FDG PET/CT. Ann Nucl Med. 2021;35:485–92. 10.1007/s12149-021-01588-6. [PubMed: 33550515]
13. Karakatsanis NA, Casey ME, Lodge MA, Rahmim A, Zaidi H. Whole-body direct 4D parametric PET imaging employing nested generalized Patlak expectation–maximization reconstruction. Phys Med Biol. 2016;61:5456. [PubMed: 27383991]
14. Karakatsanis NA, Garibotto V, Rager O, Zaidi H. Continuous bed motion vs. step-and-shoot acquisition on clinical whole-body dynamic and parametric PET imaging. In: Conference Record of the 2015 IEEE Nuclear Science Symposium and Medical Imaging Conference. Piscataway, NJ: IEEE; 2015. pp. 1–6.
15. Surti S, Pantel AR, Karp JS. Total body PET: why, how, what for? TRPMS. 2020;4:283–92.
16. Viswanath V, Pantel AR, Daube-Witherspoon ME, Doot R, Muzi M, Mankoff DA, et al. Quantifying bias and precision of kinetic parameter estimation on the PennPET Explorer, a long axial field-of-view scanner. IEEE Trans Radiat Plasma Med Sci. 2020;4:735–49. 10.1109/trpms.2020.3021315. [PubMed: 33225120]
17. Spencer BA, Berg E, Schmall JP, Omidvari N, Leung EK, Abdelhafez YG, et al. Performance evaluation of the uEXPLORER total-body PET/CT scanner based on NEMA NU 2–2018 with additional tests to characterize PET scanners with a long axial field-of-view. J Nucl Med. 2021;62:861–70. 10.2967/jnumed.120.250597. [PubMed: 33008932]
18. Viswanath V, Daube-Witherspoon ME, Pantel AR, Parma MJ, Werner ME, Karp JS. Performance benefits of extending the AFOV of PET scanners. n: Conference Record of the 2020 IEEE Nuclear Science Symposium and Medical Imaging Conference. Piscataway, NJ: IEEE; 2020. pp. 1–7.
19. Prenosil GA, Sari H, Fürstner M, Afshar-Oromieh A, Shi K, Rominger A, et al. Performance characteristics of the Biograph Vision Quadra PET/CT system with long axial field of view using the NEMA NU 2–2018 standard. J Nucl Med. 2021. 10.2967/jnumed.121.261972.
20. Zhang X, Xie Z, Berg E, Judenhofer MS, Liu W, Xu T, et al. Total-body dynamic reconstruction and parametric imaging on the uEXPLORER. J Nucl Med. 2020;61:285–91. [PubMed: 31302637]
21. Wang G, Nardo L, Parikh M, Lara P, Spencer B, Qi J, et al. Simultaneous imaging of cancer and heart using total-body multiparametric PET on EXPLORER. J Nucl Med. 2021;62(suppl. 1):1447. [PubMed: 34272322]
22. Wang Y, Cherry S, Badawi R, Wang G. Effect of dual-input function and dispersion on lung FDG-PET kinetic quantification using the EXPLORER total-body PET/CT scanner. J Nucl Med. 2020;61(suppl. 1):13. [PubMed: 31712326]

23. Sari H, Hong J, Eriksson L, Shi K, Conti M, Alberts I, et al. Kinetic modelling of dynamic ^{18}F-FDG datasets from long axial field-of-view PET scanner. J Nucl Med. 2021;62(suppl. 1):1405.
24. Strauss LG, Pan L, Cheng C, Haberkorn U, Dimitrakopoulou-Strauss A. Shortened acquisition protocols for the quantitative assessment of the 2-tissue-compartment model using dynamic PET/CT 18F-FDG studies. J Nucl Med. 2011;52:379–85. 10.2967/jnumed.110.079798. [PubMed: 21321263]
25. Wu Y, Feng T, Zhao Y, Xu T, Fu F, Huang Z, et al. Whole-body parametric imaging of FDG PET using uEXPLORER with reduced scan time. J Nucl Med. 2021. 10.2967/jnumed.120.261651.
26. Sari H, Mingels C, Alberts I, Hu J, Buesser D, Shah V, et al. First results on kinetic modelling and parametric imaging of dynamic ^{18}F-FDG datasets from a long-axial FOV PET scanner in oncological patients. Eur J Nucl Med Mol Imaging. 2022;(0123456789). 10.1007/s00259-021-05623-6.
27. Boellaard R, Delgado-Bolton R, Oyen WJ, Giammarile F, Tatsch K, Eschner W, et al. FDG PET/CT: EANM procedure guidelines for tumour imaging: version 2.0. Eur J Nucl Med Mol Imaging. 2015;42:328–54. 10.1007/s00259-014-2961-x. [PubMed: 25452219]
28. Cheng G, Torigian DA, Zhuang H, Alavi A. When should we recommend use of dual time-point and delayed time-point imaging techniques in FDG PET? Eur J Nucl Med Mol imaging. 2013;40:779–87. [PubMed: 23361859]
29. Dimitrakopoulou-Strauss A, Pan L, Sachpekidis C. Kinetic modeling and parametric imaging with dynamic PET for oncological applications: general considerations, current clinical applications, and future perspectives. Eur J Nucl Med Mol Imaging. 2021;48:21–39. [PubMed: 32430580]
30. Patlak CS, Blasberg RG. Graphical evaluation of blood-to-brain transfer constants from multiple-time uptake data. Generalizations. J Cereb Blood Flow Metab. 1985;5:584–90. [PubMed: 4055928]
31. PMOD Kinetic Modeling Toolkit (PKIN). https://www.pmod.com/files/download/v31/doc/pkin/2326.htm. Accessed 04 Feb 2022.
32. Minn H, Zasadny KR, Quint LE, Wahl RL. Lung cancer: reproducibility of quantitative measurements for evaluating 2-[F-18]-fluoro-2-deoxy-D-glucose uptake at PET. Radiol. 1995;196:167–73.
33. Dimitrakopoulou-Strauss A, Strauss LG, Burger C, Rühl A, Irngartinger G, Stremmel W, et al. Prognostic aspects of ^{18}F-FDG PET kinetics in patients with metastatic colorectal carcinoma receiving FOLFOX chemotherapy. J Nucl Med. 2004;45:1480–7. [PubMed: 15347714]
34. Dimitrakopoulou-Strauss A, Georgoulias V, Eisenhut M, Herth F, Koukouraki S, Mäcke HR, et al. Quantitative assessment of SSTR2 expression in patients with non-small cell lung cancer using ^{68}Ga-DOTATOC PET and comparison with ^{18}F-FDG PET. Eur J Nucl Med Mol Imaging. 2006;33:823–30. [PubMed: 16570185]
35. Graham M, Peterson L, Hayward R. Comparison of simplified quantitative analyses of FDG uptake. Nucl Med Biol. 2000;27:647–55. [PubMed: 11091107]
36. Alberts I, Hünermund J-N, Prenosil G, Mingels C, Bohn KP, Viscione M, et al. Clinical performance of long axial field of view PET/CT: a head-to-head intra-individual comparison of the Biograph Vision Quadra with the Biograph Vision PET/CT. Eur J Nucl Med Mol Imaging. 2021:1–10.
37. McCready VR, Dizdarevic S, Beyer T. Lesion detection and administered activity. J Nucl Med. 2020;61:1406–10. [PubMed: 32245895]
38. Li Y, Matej S, Karp JS. Practical joint reconstruction of activity and attenuation with autonomous scaling for time-of-flight PET. Phys Med Biol. 2020;65:235037. [PubMed: 32340014]
39. Teimoorisichani M, Panin V, Rothfuss H, Sari H, Rominger A, Conti M. A CT-less approach to quantitative PET imaging using the LSO intrinsic radiation for long-axial FOV PET scanners. Med Phys. 2021. 10.1002/mp.15376.
40. Rahmim A, Rousset O, Zaidi H. Strategies for motion tracking and correction in PET. PET Clin. 2007;2:251–66. 10.1016/j.cpet.2007.08.002. [PubMed: 27157876]
41. Ren S, Lu Y, Bertolli O, Thielemans K, Carson RE. Event-by-event non-rigid data-driven PET respiratory motion correction methods: comparison of principal component analysis and

centroid of distribution. Phys Med Biol. 2019;64:165014. 10.1088/1361-6560/ab0bc9. [PubMed: 30822762]

42. Badawi RD, Shi H, Hu P, Chen S, Xu T, Price PM, et al. First human imaging studies with the EXPLORER total-body PET scanner. J Nucl Med. 2019;60:299–303. [PubMed: 30733314]
43. Alberts I, Sachpekidis C, Dijkstra L, Prenosil G, Gourni E, Boxler S, et al. The role of additional late PSMA-ligand PET/CT in the differentiation between lymph node metastases and ganglia. Eur J Nucl Med Mol Imaging. 2020;47:642–51. 10.1007/s00259-019-04552-9. [PubMed: 31865408]

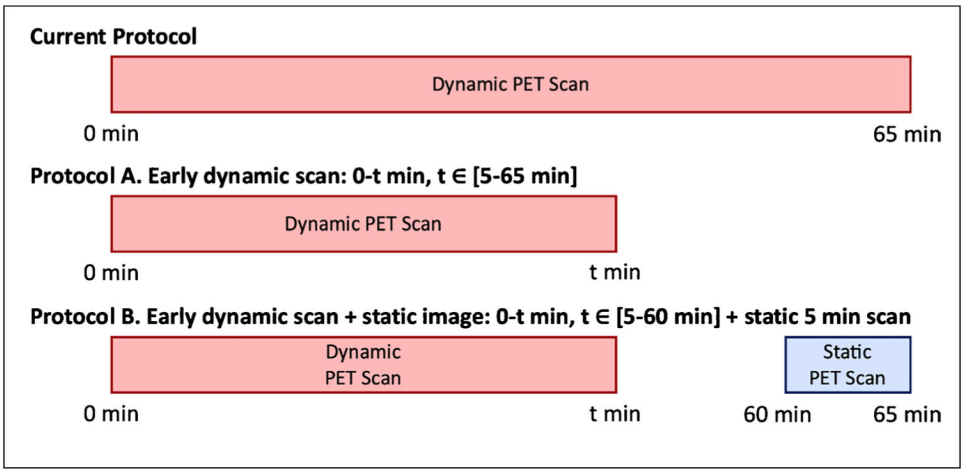

Fig. 1.

Schematic of the current dynamic imaging protocol for ^{18}F-FDG (top), along with the two proposed abbreviated scan protocols: Protocol **A**: early dynamic imaging only (middle); and Protocol **B**: early dynamic imaging plus a static scan

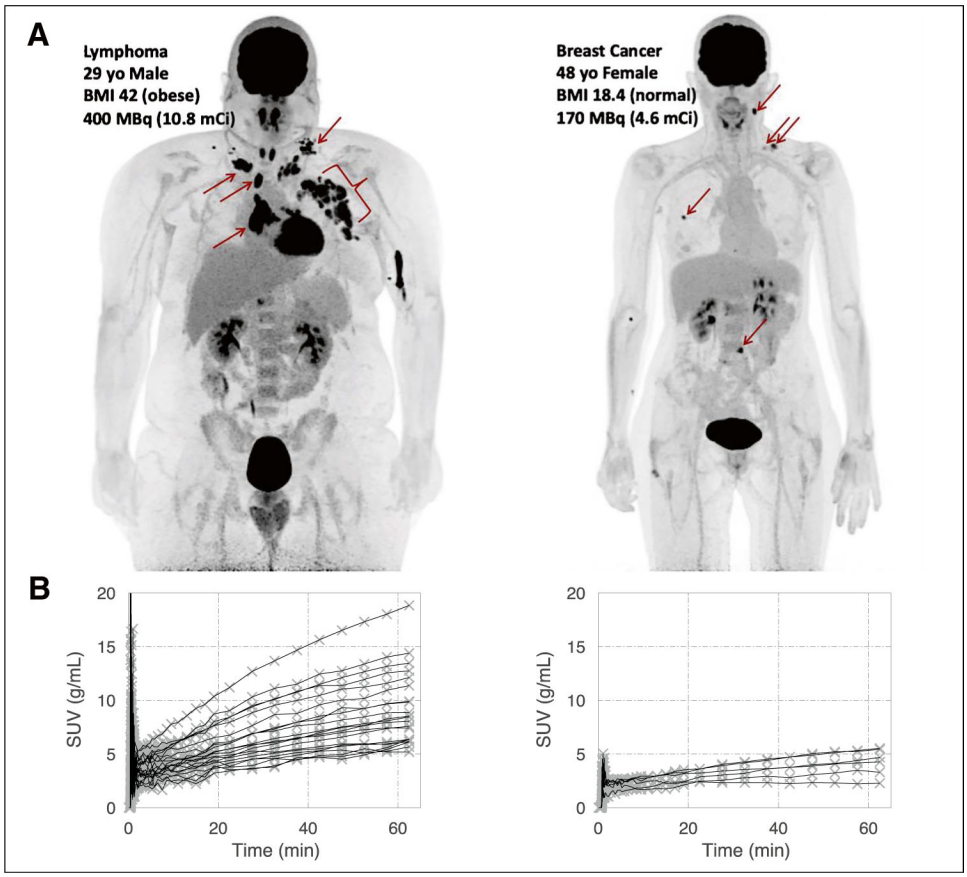

Fig. 2.

A Example maximum intensity projection SUV images of 5-min duration (60–65 min p.i.) for two representative patients with lymphoma (left) and breast cancer (right). Color scale is SUV 0–5. **B** shows TAC from all lesions from the representative patients. Note that the mass of lesions indicated in the lymphoma patient was separated for analysis into many smaller individual lesions, whose TAC are shown in **B**

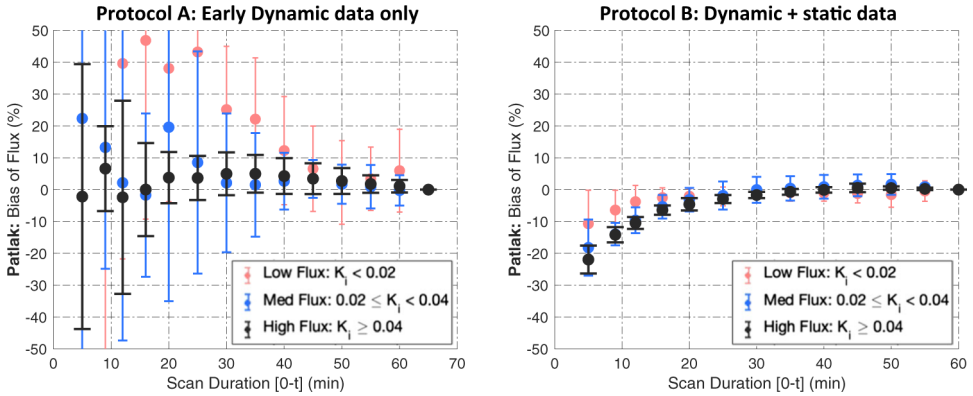

Fig. 3.

Bias of flux estimated using Patlak graphical analysis as a function of dynamic scan duration for both abbreviated scan protocols

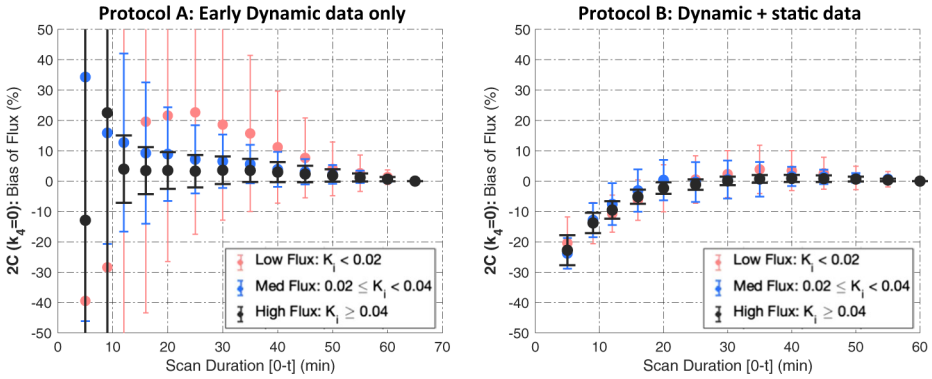

Fig. 4.

Bias of flux estimated using an irreversible two-tissue-compartment model as a function of dynamic scan duration for both abbreviated scan protocols

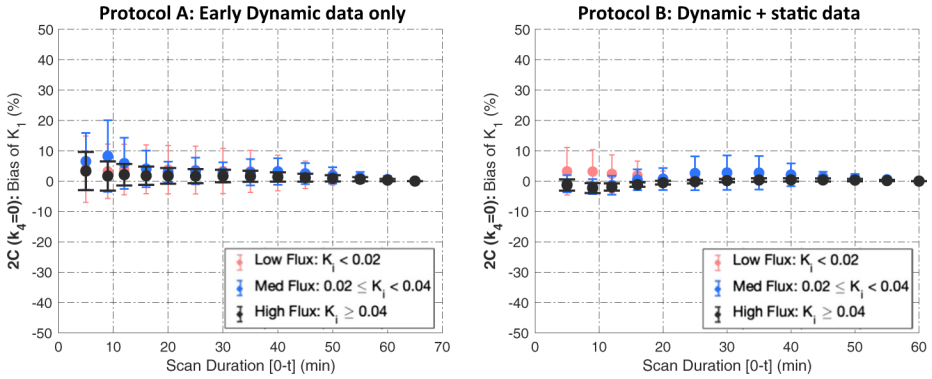

Fig. 5.

Bias of delivery (K_1) estimated using an irreversible two-tissue-compartment model as a function of dynamic scan duration for both abbreviated scan protocols

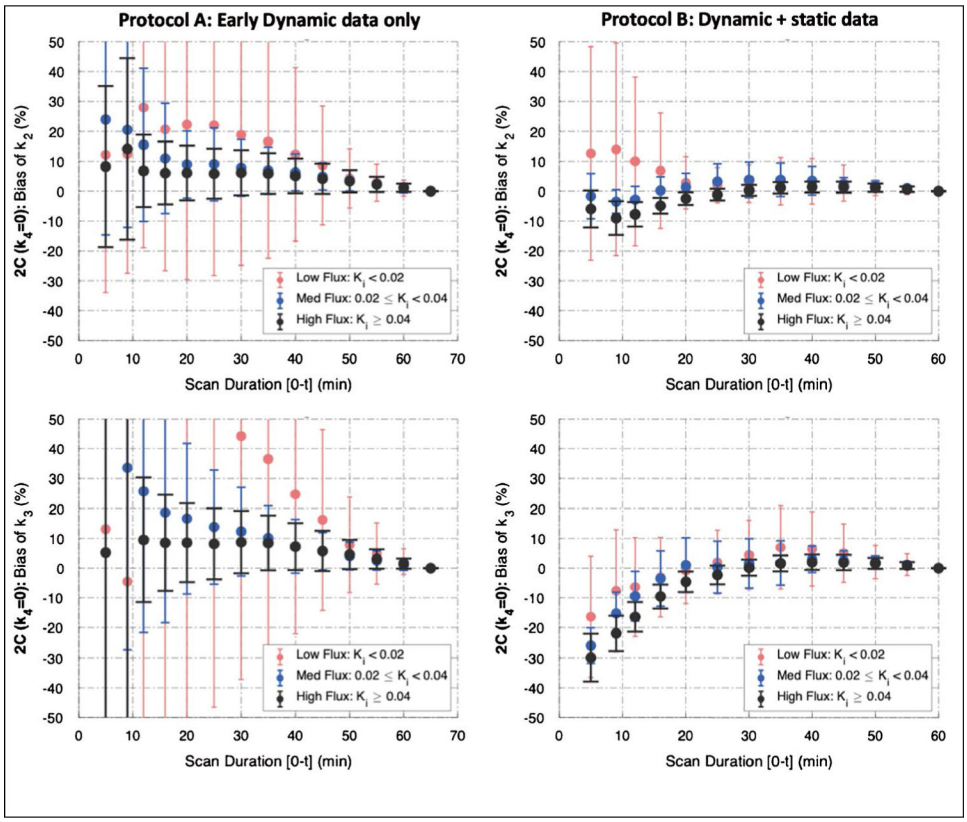

Fig. 6.

Bias and precision of microparameters k_2 (top) and k_3 (bottom), estimated using a 2-tissue-compartment model using both protocol A (left) and protocol B (right)

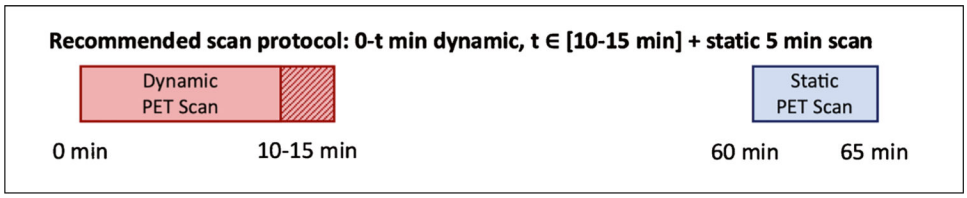

Fig. 7.
Recommended scan protocol

Table 1

Patient demographics ($N = 9$)

Age	29–77 years
Gender	6 MI3 F
Weight	52–130 kg
Injected activity	170–400 MBq (4.6–10.8 mCi)
Number of hypermetabolic lesions	Lymphoma: 25 (in 3 pts.) Breast Ca: 11 (in 3 pts.) Lung Ca: 2 (in 2 pts.) Gastric Cancer: 1 (in 1 pt.)

Table 2

Scan durations at which bias or precision of flux exceeds 10%

	Protocol A: Early dynamic data only		Protocol B: dynamic + static data	
	***Bias* > 10%**	***Precision* > 10%**	***Bias* > 10%**	***Precision* > 10%**
A. Patlak graphical analysis				
Low flux (*N* = 8)	42 min	55 min	6 min	5 min
Medium flux (*N* = 18)	24 min	39 min	12 min	< 5 min
High flux (*N* = 13)	< 5 min	16 min	12 min	< 5 min
B. Two-tissue-compartment model				
Low flux (*N* = 8)	42 min	49 min	13 min	< 5 min
Medium flux (*N* = 15)	15 min	28 min	11 min	< 5 min
High flux (*N* = 16)	11 min	13 min	12 min	< 5 min

Table 3

Scan durations at which bias or precision of flux exceeds different thresholds

Threshold	5%	7.5%	10%	12.5%
Patlak graphical analysis - protocol A				
Low flux (N = 8)	58 min (60 min)[a]	44 min (57 min)	42 min (55 min)	40 min (59 min)
Medium flux (N = 18)	39 min (57 min)	29 min (50 min)	20 min (39 min)	12 min (38 min)
High flux (N = 13)	35 min (44 min)	< 5 min (22 min)	< 5 min (16 min)	< 5 min (11 min)
Patlak graphical analysis - protocolB				
Low flux (N = 8)	11 min (15 min)	8 min (8 min)	6 min (5 min)	< 5 min (< 5 min)
Medium flux (N = 18)	17 min (22 min)	14 min (11 min)	12 min (< 5 min)	10 min (< 5 min)
High flux (N = 13)	19 min (< 5 min)	15 min (< 5 min)	12 min (< 5 min)	10 min (< 5 min)
Two-tissue-compartment model - protocol A				
Low flux (N = 8)	49 min (56 min)	45 min (52 min)	42 min (49 min)	39 min (46 min)
Medium flux (N = 15)	37 min (42 min)	24 min (33 min)	15 min (28 min)	12 min (23 min)
High flux (N = 16)	12 min (27 min)	11 min (17 min)	11 min (13 min)	11 min (12 min)
Two-tissue-compartment model - protocol B				
Low flux (N = 8)	17 min (46 min)	15 min (25 min)	13 min (< 5 min)	10 min (< 5 min)
Medium flux (N = 15)	14 min (6 min)	12 min (< 5 min)	11 min (< 5 min)	9 min (< 5 min)
High flux (N = 16)	16 min (< 5 min)	14 min (< 5 min)	12 min (< 5 min)	10 min (< 5 min)

[a]Scan duration for which the bias (precision) exceeds the threshold

Table 4

Scan durations at which bias and precision of k_2 and k_3 exceeds 10%

	Protocol A: early dynamic data only		Protocol B: dynamic + static data	
	Bias > 10%	***Precision > 10%***	***Bias > 10%***	***Precision > 10%***
A. k_2: efflux from the first compartment				
Low flux	43 min	50 min	12 min	20 min
Medium flux	18 min	36 min	< 5 min	< 5 min
High flux	11 min	17 min	< 5 min	< 5 min
B. k_3: phosphorylation of ^{18}F-FDG				
Low flux	49 min	55 min	8 min	45 min
Medium flux	35 min	37 min	12 min	< 5 min
High flux	12 min	32 min	16 min	< 5 min